Supplement of Biogeosciences Discuss., 12, 8157–8197, 2015
http://www.biogeosciences-discuss.net/12/8157/2015/
doi:10.5194/bgd-12-8157-2015-supplement

Supplement of

A latitudinally-banded phytoplankton response to 21st century climate change in the Southern Ocean across the CMIP5 model suite

S. Leung et al.

Correspondence to: S. Leung (shirlleu@uw.edu)

Model	*Scenario*	*30-40°S*	*40-50°S*	*50-65°S*	*S of 65°S*	*Total*
CanESM2	*hist*	49.005	103.100	47.209	8.503	207.817
	rcp8.5	39.825	97.357	51.527	14.324	203.033
	delta	**-9.180**	**-5.743**	**4.318**	**5.821**	**-4.784**
	rel delta	**-18.73%**	**-5.57%**	**9.15%**	**68.46%**	**-2.30%**
CESM1-BGC	*hist*	54.855	191.250	265.320	157.770	669.195
	rcp8.5	47.063	151.320	213.480	158.580	570.443
	delta	**-7.792**	**-39.930**	**-51.840**	**0.810**	**-98.752**
	rel delta	**-14.20%**	**-20.88%**	**-19.54%**	**0.51%**	**-14.76%**
GFDL-ESM2G	*hist*	102.850	126.380	140.940	74.096	444.266
	rcp8.5	99.233	130.100	140.910	76.512	446.755
	delta	**-3.617**	**3.720**	**-0.030**	**2.416**	**2.489**
	rel delta	**-3.52%**	**2.94%**	**-0.02%**	**3.26%**	**0.56%**
GFDL-ESM2M	*hist*	118.980	128.190	159.780	88.524	495.474
	rcp8.5	114.220	132.160	153.610	92.679	492.669
	delta	**-4.760**	**3.970**	**-6.170**	**4.155**	**-2.805**
	rel delta	**-4.00%**	**3.10%**	**-3.86%**	**4.69%**	**-0.57%**
HadGEM2-CC	*hist*	262.510	471.880	530.110	147.850	1412.350
	rcp8.5	220.690	483.040	494.730	177.540	1376.000
	delta	**-41.820**	**11.160**	**-35.380**	**29.690**	**-36.350**
	rel delta	**-15.93%**	**2.37%**	**-6.67%**	**20.08%**	**-2.57%**
HadGEM2-ES	*hist*	259.410	458.830	478.690	135.000	1331.930
	rcp8.5	215.440	479.700	466.980	170.350	1332.470
	delta	**-43.970**	**20.870**	**-11.710**	**35.350**	**0.540**
	rel delta	**-16.95%**	**4.55%**	**-2.45%**	**26.19%**	**0.04%**
IPSL-CM5A-LR	*hist*	103.880	104.970	147.820	82.455	439.125
	rcp8.5	86.633	96.955	136.510	89.627	409.725
	delta	**-17.247**	**-8.015**	**-11.310**	**7.172**	**-29.400**
	rel delta	**-16.60%**	**-7.64%**	**-7.65%**	**8.70%**	**-6.70%**
IPSL-CM5A-MR	*hist*	100.580	103.320	131.360	80.698	415.958
	rcp8.5	81.935	102.870	128.610	86.796	400.211
	delta	**-18.645**	**-0.450**	**-2.750**	**6.098**	**-15.747**
	rel delta	**-18.54%**	**-0.44%**	**-2.09%**	**7.56%**	**-3.79%**
MPI-ESM-LR	*hist*	382.460	854.660	1841.700	768.960	3847.780
	rcp8.5	310.530	923.440	1629.000	841.910	3704.880
	delta	**-71.930**	**68.780**	**-212.700**	**72.950**	**-142.900**
	rel delta	**-18.81%**	**8.05%**	**-11.55%**	**9.49%**	**-3.71%**
MPI-ESM-MR	*hist*	313.000	870.370	1881.200	731.740	3796.310
	rcp8.5	270.730	888.010	1762.300	788.220	3709.260
	delta	**-42.270**	**17.640**	**-118.900**	**56.480**	**-87.050**
	rel delta	**-13.50%**	**2.03%**	**-6.32%**	**7.72%**	**-2.29%**
MRI-ESM1	*hist*	64.063	68.103	76.655	25.450	234.271
	rcp8.5	62.270	70.676	75.273	25.507	233.726
	delta	**-1.793**	**2.573**	**-1.382**	**0.057**	**-0.545**
	rel delta	**-2.80%**	**3.78%**	**-1.80%**	**0.22%**	**-0.23%**
NorESM1-ME	*hist*	374.630	696.240	797.840	147.620	2016.330
	rcp8.5	317.070	734.930	725.870	218.070	1995.940
	delta	**-57.560**	**38.690**	**-71.970**	**70.450**	**-20.390**
	rel delta	**-15.36%**	**5.56%**	**-9.02%**	**47.72%**	**-1.01%**
GISS-E2-H-CC	*hist*	41.006	167.710	431.630	159.420	799.766
	rcp8.5	32.961	144.990	391.390	213.780	783.121
	delta	**-8.045**	**-22.720**	**-40.240**	**54.360**	**-16.645**
	rel delta	**-19.62%**	**-13.55%**	**-9.32%**	**34.10%**	**-2.08%**
GISS-E2-R-CC	*hist*	68.378	101.910	251.800	160.360	582.448
	rcp8.5	53.751	103.600	216.500	198.110	571.961
	delta	**-14.627**	**1.690**	**-35.300**	**37.750**	**-10.487**
	rel delta	**-21.39%**	**1.66%**	**-14.02%**	**23.54%**	**-1.80%**
All-model means	*hist*	163.972	317.637	513.004	197.746	1192.359
	rcp8.5	139.454	324.225	470.478	225.143	1159.300
	delta	**-24.518**	**6.588**	**-42.526**	**27.397**	**-33.059**
	rel delta	**-14.95%**	**2.07%**	**-8.29%**	**13.85%**	**-2.77%**

Table S1: Surface phytoplankton biomass concentrations (PB) across the CMIP5 models. PB spatially averaged over each zonal band within each model for the *historical* (1980-99 average) and *rcp8.5* (2080-99 average) simulations. Rows labeled "delta" list 100-year absolute changes (*rcp8.5* minus *historical*) in PB, while rows labeled "rel delta" list 100-year relative changes (absolute change in PB over *historical* PB). Units are mmol m^{-3} phytoplankton concentration.

Model	*Scenario*	*30-40°S*	*40-50°S*	*50-65°S*	*S of 65°S*	*Total*
CanESM2	*hist*	2.133	5.380	0.945	0.073	8.531
	rcp8.5	1.460	5.549	1.129	0.124	8.260
	delta	**-0.673**	**0.168**	**0.184**	**0.051**	**-0.271**
	rel delta	**-31.57%**	**3.13%**	**19.45%**	**69.73%**	**-3.17%**
CESM1-BGC	*hist*	4.988	4.440	3.084	0.483	12.995
	rcp8.5	4.819	4.755	3.335	0.590	13.499
	delta	**-0.169**	**0.315**	**0.251**	**0.107**	**0.505**
	rel delta	**-3.38%**	**7.10%**	**8.15%**	**22.19%**	**3.89%**
CMCC-CESM	*hist*	4.829	2.599	2.648	0.359	10.434
	rcp8.5	4.699	2.890	2.892	0.457	10.938
	delta	**-0.130**	**0.291**	**0.244**	**0.099**	**0.504**
	rel delta	**-2.70%**	**11.21%**	**9.22%**	**27.54%**	**4.83%**
GFDL-ESM2G	*hist*	6.194	5.330	4.150	0.976	16.650
	rcp8.5	6.307	5.577	3.980	0.973	16.837
	delta	**0.113**	**0.247**	**-0.170**	**-0.003**	**0.187**
	rel delta	**1.82%**	**4.64%**	**-4.09%**	**-0.32%**	**1.12%**
GFDL-ESM2M	*hist*	7.793	5.971	4.700	1.164	19.628
	rcp8.5	7.994	6.253	4.567	1.176	19.990
	delta	**0.201**	**0.282**	**-0.133**	**0.012**	**0.362**
	rel delta	**2.58%**	**4.72%**	**-2.83%**	**1.04%**	**1.84%**
HadGEM2-CC	*hist*	3.811	6.339	5.900	1.028	17.079
	rcp8.5	3.036	6.043	5.804	1.378	16.261
	delta	**-0.775**	**-0.296**	**-0.096**	**0.350**	**-0.817**
	rel delta	**-20.34%**	**-4.67%**	**-1.62%**	**33.99%**	**-4.79%**
HadGEM2-ES	*hist*	3.708	6.153	5.651	0.919	16.431
	rcp8.5	2.993	5.982	5.658	1.325	15.958
	delta	**-0.716**	**-0.170**	**0.007**	**0.405**	**-0.474**
	rel delta	**-19.29%**	**-2.77%**	**0.13%**	**44.05%**	**-2.88%**
IPSL-CM5A-LR	*hist*	4.624	3.409	2.650	0.599	11.282
	rcp8.5	4.242	3.641	2.690	0.678	11.250
	delta	**-0.382**	**0.232**	**0.040**	**0.079**	**-0.032**
	rel delta	**-8.26%**	**6.80%**	**1.51%**	**13.13%**	**-0.28%**
IPSL-CM5A-MR	*hist*	4.403	3.462	2.650	0.634	11.149
	rcp8.5	4.021	3.867	2.705	0.700	11.293
	delta	**-0.382**	**0.405**	**0.055**	**0.066**	**0.144**
	rel delta	**-8.67%**	**11.69%**	**2.08%**	**10.40%**	**1.29%**
MIROC-ESM-CHEM	*hist*	4.297	4.539	2.891	0.284	12.011
	rcp8.5	3.650	4.991	3.059	0.519	12.218
	delta	**-0.647**	**0.452**	**0.168**	**0.235**	**0.207**
	rel delta	**-15.06%**	**9.96%**	**5.80%**	**82.63%**	**1.72%**
MPI-ESM-LR	*hist*	5.157	7.269	8.027	1.603	22.055
	rcp8.5	4.296	7.350	7.421	1.951	21.017
	delta	**-0.862**	**0.081**	**-0.605**	**0.348**	**-1.038**
	rel delta	**-16.71%**	**1.12%**	**-7.54%**	**21.70%**	**-4.71%**
MPI-ESM-MR	*hist*	4.406	7.145	8.161	1.569	21.281
	rcp8.5	3.922	7.289	7.969	1.743	20.923
	delta	**-0.484**	**0.145**	**-0.192**	**0.174**	**-0.357**
	rel delta	**-10.98%**	**2.02%**	**-2.35%**	**11.07%**	**-1.68%**
MRI-ESM1	*hist*	2.842	3.095	1.897	0.215	8.048
	rcp8.5	2.690	3.416	2.123	0.291	8.521
	delta	**-0.151**	**0.322**	**0.226**	**0.076**	**0.473**
	rel delta	**-5.32%**	**10.39%**	**11.92%**	**35.55%**	**5.87%**
NorESM1-ME	*hist*	3.965	6.959	4.385	0.346	15.655
	rcp8.5	3.276	7.048	4.595	0.497	15.416
	delta	**-0.689**	**0.090**	**0.210**	**0.151**	**-0.239**
	rel delta	**-17.37%**	**1.29%**	**4.78%**	**43.57%**	**-1.52%**
GISS-E2-H-CC	*hist*	0.466	2.655	2.468	0.325	5.914
	rcp8.5	0.428	2.677	2.921	0.436	6.462
	delta	**-0.037**	**0.023**	**0.452**	**0.110**	**0.547**
	rel delta	**-8.02%**	**0.85%**	**18.32%**	**33.82%**	**9.26%**
GISS-E2-R-CC	*hist*	1.776	2.935	2.835	0.550	8.097
	rcp8.5	1.211	3.131	2.935	0.676	7.954
	delta	**-0.565**	**0.196**	**0.100**	**0.126**	**-0.143**
	rel delta	**-31.80%**	**6.69%**	**3.52%**	**22.84%**	**-1.77%**
All-model means	*hist*	4.162	4.847	4.215	0.755	13.980
	rcp8.5	3.769	5.011	4.237	0.914	13.931
	delta	**-0.393**	**0.164**	**0.022**	**0.159**	**-0.048**
	rel delta	**-9.45%**	**3.39%**	**0.52%**	**21.06%**	**-0.35%**

Table S2: 100-m vertically-integrated primary productivity rates (PP) across the CMIP5 models. PP spatially integrated over each zonal band within each model for the *historical* (1980-99 average) and *rcp8.5* (2080-99 average) simulations. Rows labeled "delta" list 100-year absolute changes (*rcp8.5* minus *historical*) in PP, while rows labeled "rel delta" list 100-year relative changes (absolute change in PP over *historical* PP). Units are PgC yr^{-1}, or petagrams of carbon per year.

Reference	*Studied area*	*Data collection method*	*Type of biomass measured*	*Time period*	*Trend calculation method*	*Direction/magnitude of significant trends*	*Proposed driving mechanism*
Atkinson et al., 2004 (A2004)	Southwest Atlantic sector of Southern Ocean (~50-65°S,~20-60°W)	Net hauls from 9 countries	Summer krill density, which is positively correlated with chl conc	1976-2003	Spatio-temporal model at each grid cell (SW Atlantic = 10 grid cells)	**-38% per decade** in krill density	None offered to explain why chl concentrations should decrease
Lovenduski and Gruber, 2005 (LG2005)	Entire Southern Ocean, divided into 4 zones defined by fronts	SeaWiFS	Chl	1997-2004	Variables were spatially averaged over each of the 4 zones and then temporally correlated/regressed with the SAM index; no actual temporal trends were calculated	Subantarctic zone (SAZ) south of Australia (~50-60°S, ~110-140°E): **-0.06 mg m^{-2} per standard deviation of SAM**	Poleward shift of surface westerly winds during positive SAM → increased convergence and downwelling in the SAZ → deeper mixed layers and increased light limitation → decreased chl in the SAZ during positive SAM
Gregg et al., 2005 (G2005)	Global ocean	SeaWiFS	Chl	1998-2003	Pixel by pixel; clusters of pixels with significant trends were then isolated as regions of interest and data were then averaged over these regions	Small area just south of Australia (~35-55°S,~110-150°E): **+28.9% over time period of study** in chl concentrations	Increase in chl accompanied by 0.56°C increase in springtime SST; warmer SST → shallower mixed layer → less light limitation
Smith and Comiso, 2008 (SC2008)	Entire SO south of 60°S, with more in-depth analysis for 6 specific small regions	SeaWiFS	Primary production calculated from remotely-sensed ocean color, SST, PAR	1998-2006	Variables are spatially averaged over the entire SO south of 60°S or over each of the six small regions and temporally averaged both monthly and annually; simple Model I regression analyses to calculate trends	- Annual PP over the entire SO increased significantly between 1998-2006 with much of the increase confined to the months of Jan and Feb - Annually over entire SO: **+3.85 g C m^{-2} yr^{-1} decade^{-1}** - All Januaries over entire SO: **+52.01 mg C m^{-2} yr^{-1} decade^{-1}** - All Februaries over entire SO: **+32.78 mg C m^{-2} yr^{-1} decade^{-1}**	- Jan and Feb are the months of minimum sea ice concentrations, suggesting that the summer increases in PP are not directly coupled to ice retreat - Instead PP increases are forced by decreasing summer cloud cover, increased iron inputs, and/or increased water column stratification, leading to enhanced irradiance availability
Arrigo et al., 2008 (A2008)	Entire Southern Ocean south of 50°S, divided into 5 geographic sectors at specific longitudes	SeaWiFS	Primary production calculated from remotely-sensed ocean color, SST, sea ice	1997-2006	Variables are spatially averaged over each different sector; regression coefficient of production vs. year is then computed for each sector	- Ross Sea sector (south of 50°S, 160°E to 130°W): **+9 Tg C yr^{-1}** - South Indian sector (south of 50°S, 20°E to 90°E): **-4 Tg C yr^{-1}**	None offered

Montes-Hugo et al., 2009 (MH2009)	Western Antarctic Peninsula (WAP)	SeaWiFS, CZCS, in-situ shipboard data	Chl	1978-1986 to 1998-2006	Spatial average over the northern and southern WAP subregions of pixel-by-pixel differences in monthly-averaged chl concentration between 1978-1986 and 1998-2006	- Northern WAP subregion (61.8-64.5°S, 59.0-65.8°W): **-1.36 (Dec), -5.43 (Jan), -2.12 (Feb) mg m^{-3}** - Southern WAP subregion (63.8-67.8°S, 64.4-73.0°W): **+1.25 (Dec), +0.49 (Jan), +0.02 (Feb) mg m^{-3}**	- Northern WAP subregion: cloudier skies, stronger winds, decreased summer sea ice extent → deeper wind-mixing and increased light limitation during months most critical for phytoplankton growth (Dec and Jan); perhaps also because of greater advection of chl-poor waters from the Weddell Sea - Southern WAP subregion: clearer skies, weaker winds, decreased summer sea ice in areas that were previously sea ice covered most of the year → more favorable light conditions for phytoplankton growth
Johnston and Gabric, 2011 (JG2011)	Australian sector of the Southern Ocean (40-70°S, 110-160°E), divided latitudinally into 5° zones	SeaWiFS	Chl and primary production calculated from remotely-sensed ocean color, PAR, SST	1997-2007	Variables are spatially averaged over the 5° zones and temporally averaged over spring and summer months; trends in seasonal (summer and spring) time series are then estimated using the non-parametric seasonal Sen slope	- 40-45°S: **+1.2E-2 (spring) mg m^{-3} yr^{-1} and +14.6 (summer) mg C m^{-2} day^{-1} yr^{-1}** - 45-50°S: +**7.2E-3 (spring) mg m^{-3} yr^{-1} and +8.4 (summer) mg C m^{-2} day^{-1} yr^{-1}** - 55-60°S: **-2.7E-3 (spring), -2.7E-3 (summer) mg m^{-3} yr^{-1}**	- 40-50°S: none offered - 55-60°S: decreased Ekman transport of iron → lower chl concs
Takao et al., 2012 (T2012)	Indian sector of the SO (south of 30°S, 110-150°E), broken up into five frontal zones	SeaWiFS	NPP calculated from remotely-sensed ocean color, PAR, absorption	1997-2007	Variables are spatially averaged over the frontal zones and temporally averaged over seasons; trends and their significance are then estimated using the non-parametric Sen slope and the Mann-Kendall test	Polar frontal zone (PFZ) (between ~45-55°S, depending on the longitude): **-2.91 mg C m^{-2} day^{-1} yr^{-1} (summer)**	-Decreasing trend in NPP pos. correlated with decreasing diatom abundance -Shifting of ACC fronts could've led to changes in iron availability via alterations in meander-induced upwelling and/or eddy mixing -Decreasing trend in PFZ NPP and diatom abundance could've been due to decrease in iron availability or increase in zooplankton grazing pressure or complex interactions between the two
Siegel et al., 2013 (S2013)	Global ocean divided up into 3 zones separated by the two mean 15°C SST isotherms	SeaWIFS	Chl and biomass calculated from remotely-sensed ocean color, particulate backscatter, PAR, SST	1997-2010	Variables were spatially averaged over the 3 regions and temporally averaged over months; type 1 linear regression to calculate trends	SO region where mean SST < 15°C (significant only in regions ~100°E-0°E, ~40-50°S and ~112°E-45°W, ~65°S): - Chl concentration (from classic band ratio algorithm): **+0.83% per yr** - Chl concentration (with dissolved organic matter and detrital particulate matter taken into account): **+1.0981% per yr**	- Migration of boundaries between bio-optical provinces in response to regional changes in physical ocean climate

Table S3: Summary of previous studies looking at trends in phytoplankton biomass and productivity within the Southern Ocean (SO).

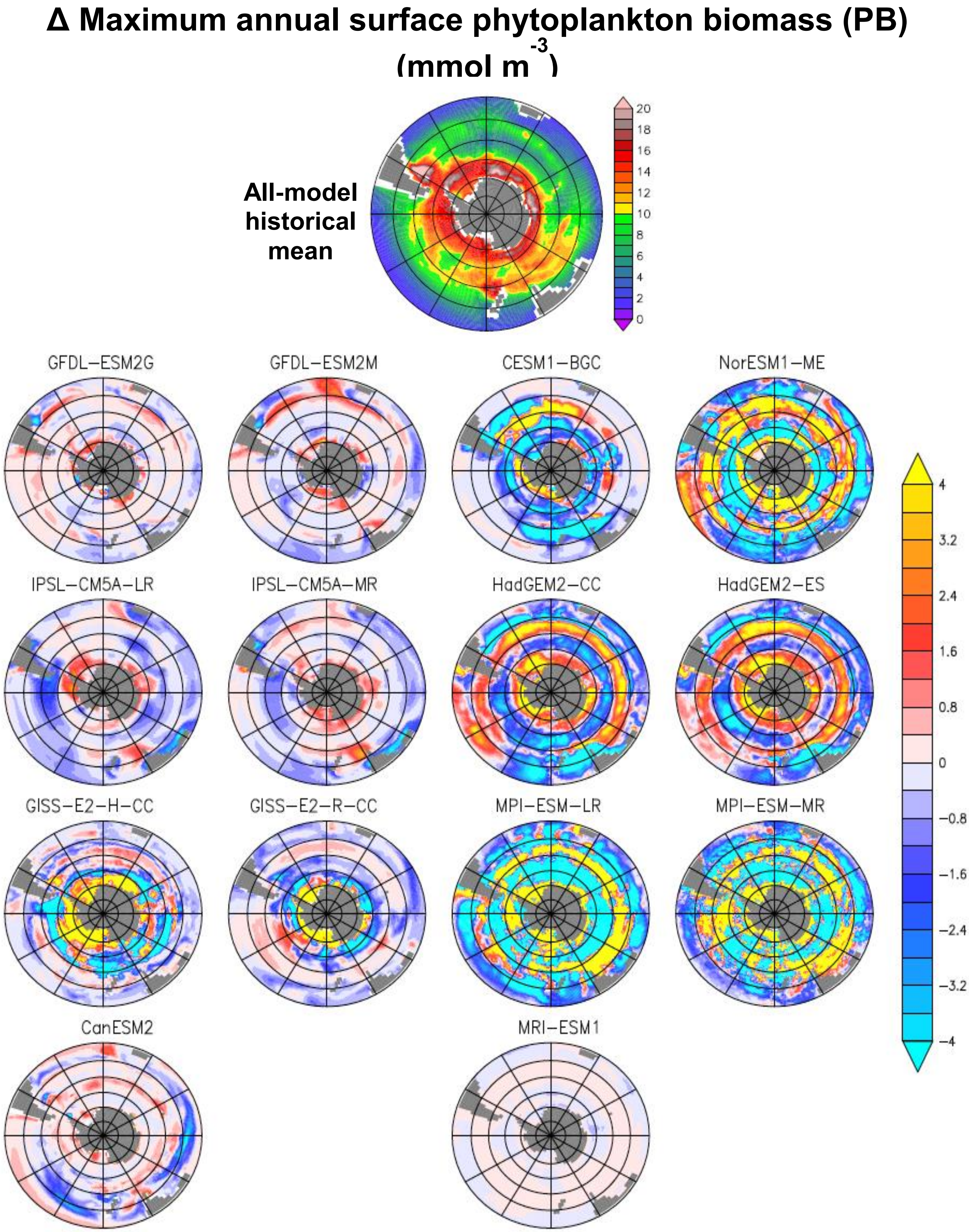

Figure S1: 100-year changes in maximum annual surface phytoplankton biomass (PB) for all the models with this data available.

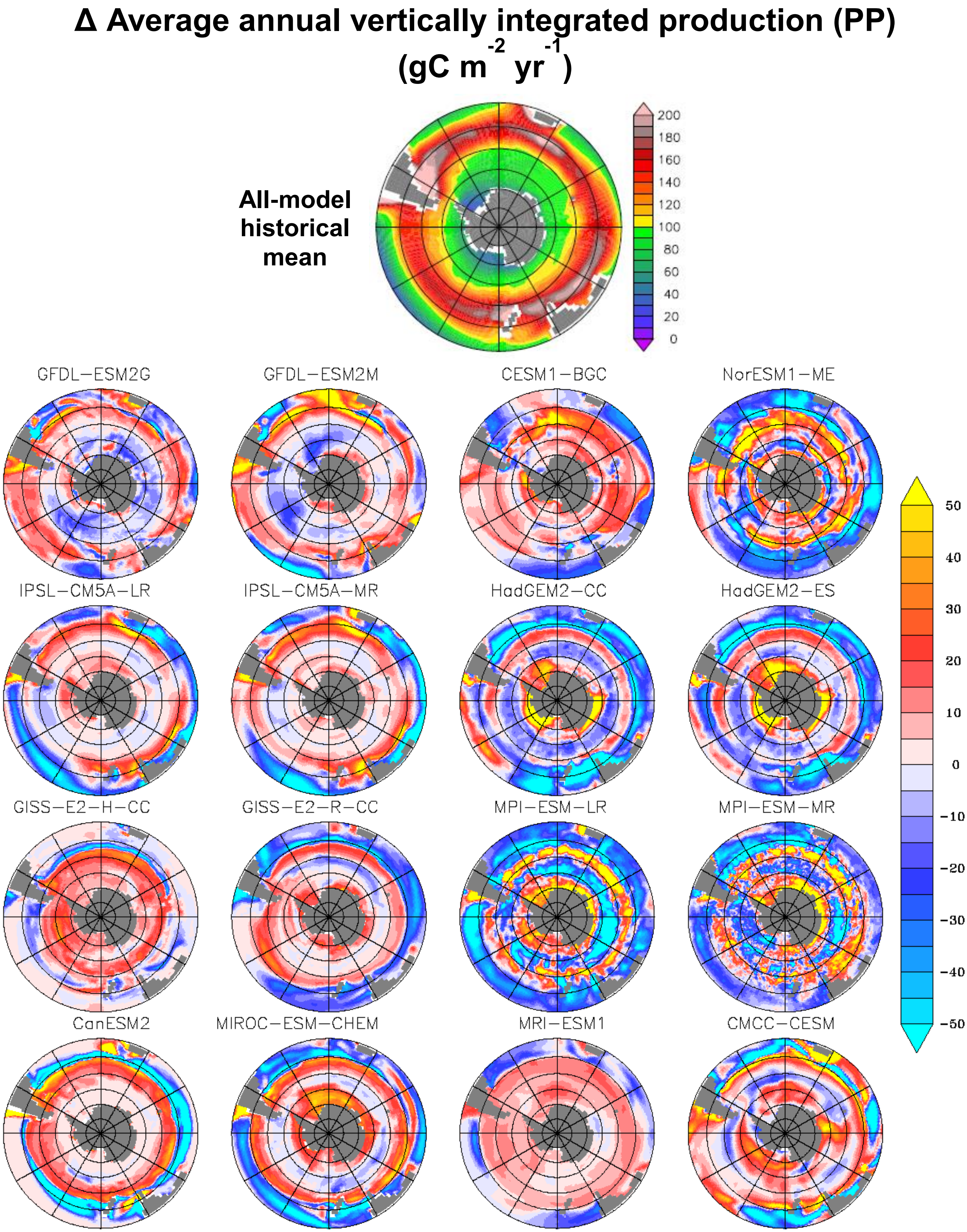

Figure S2: 100-year changes in average annual primary production integrated to 100m depth (PP) for all the models with this data available.

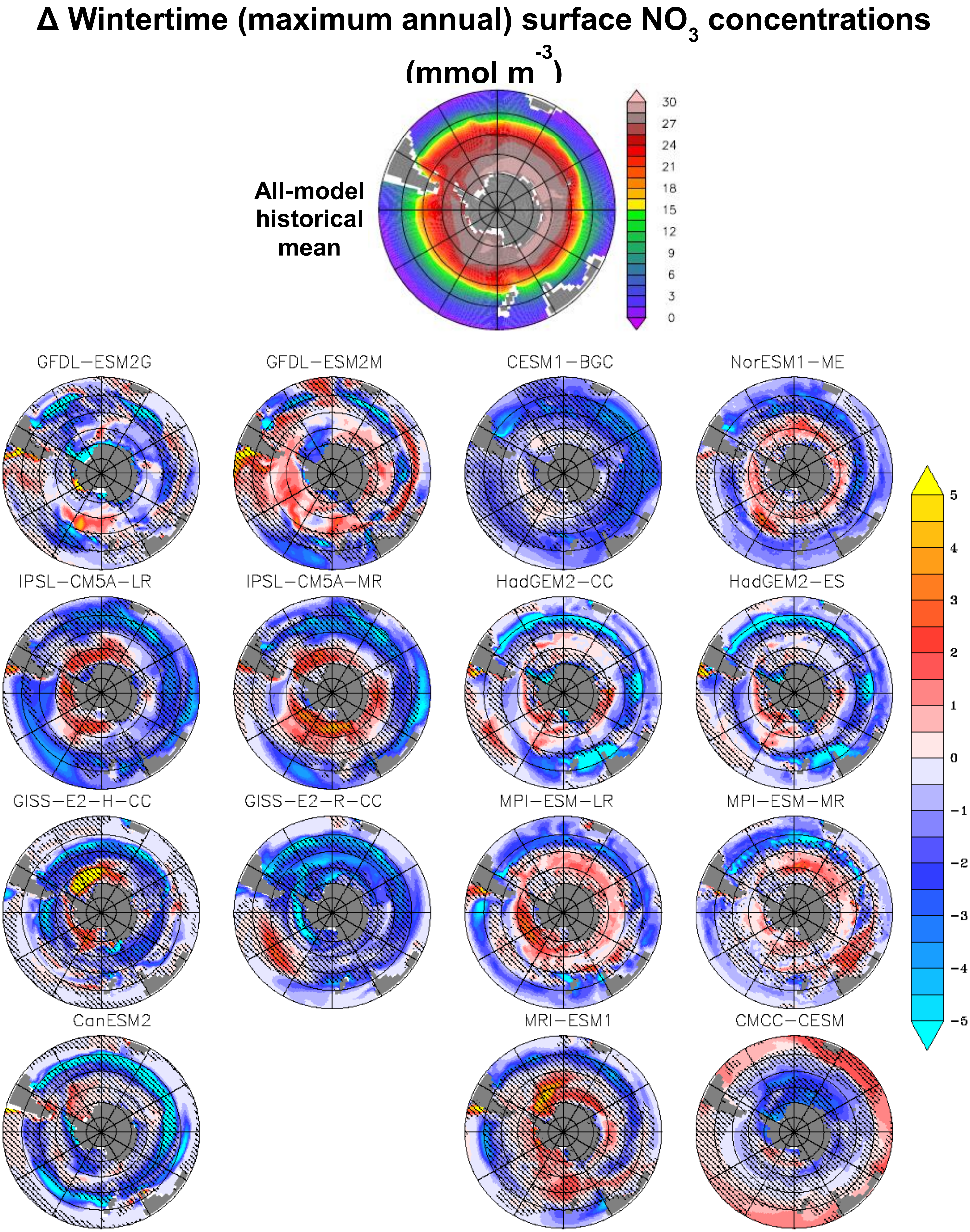

Figure S3: 100-year changes in maximum annual surface NO_3 concentration for all the models with this data available. Shaded areas are where PP increases.

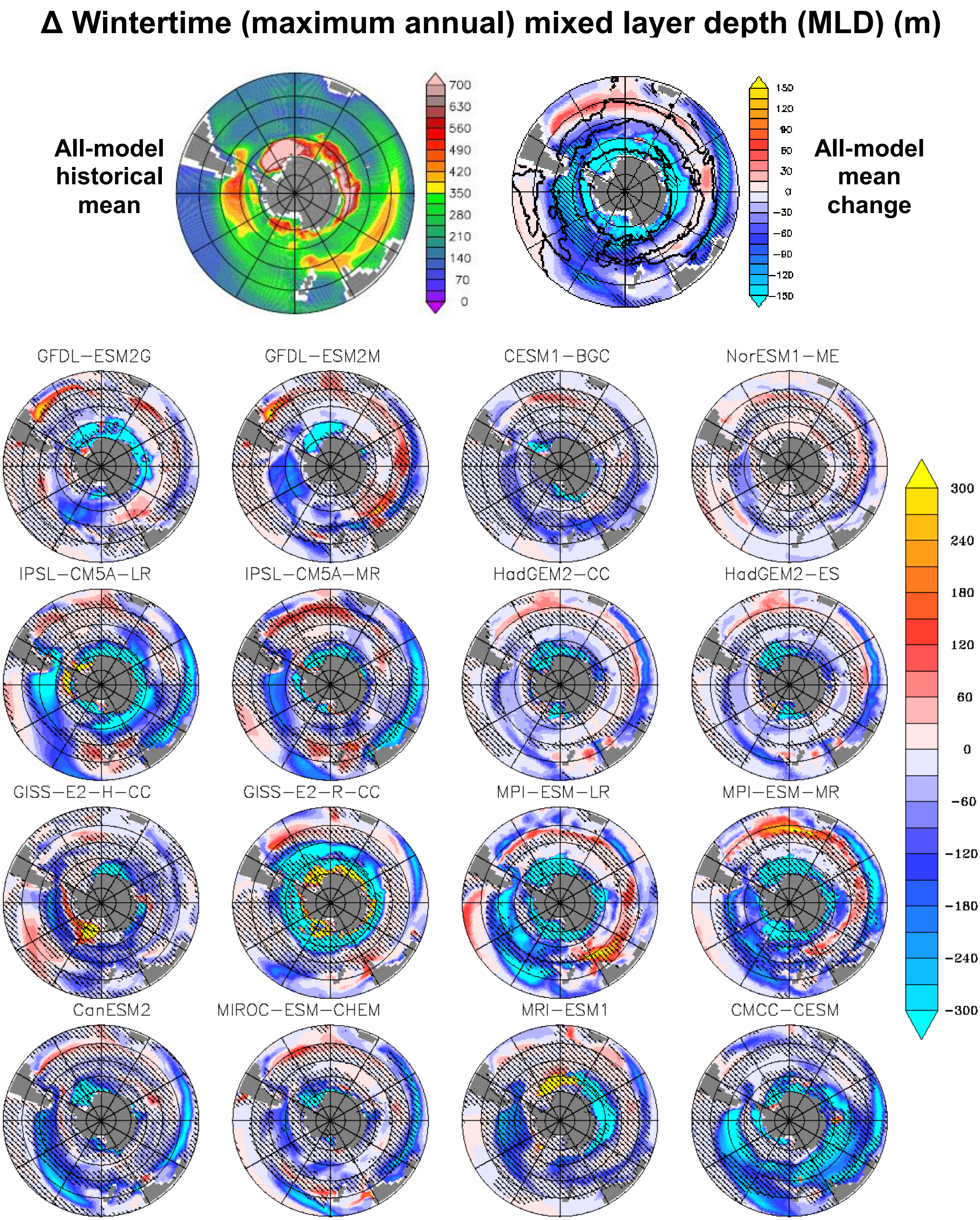

Figure S4: 100-year changes in maximum annual MLD for all the models with this data available. Shaded areas are where PP increases.

Δ Summertime (minimum annual) mixed layer depth (MLD) (m)

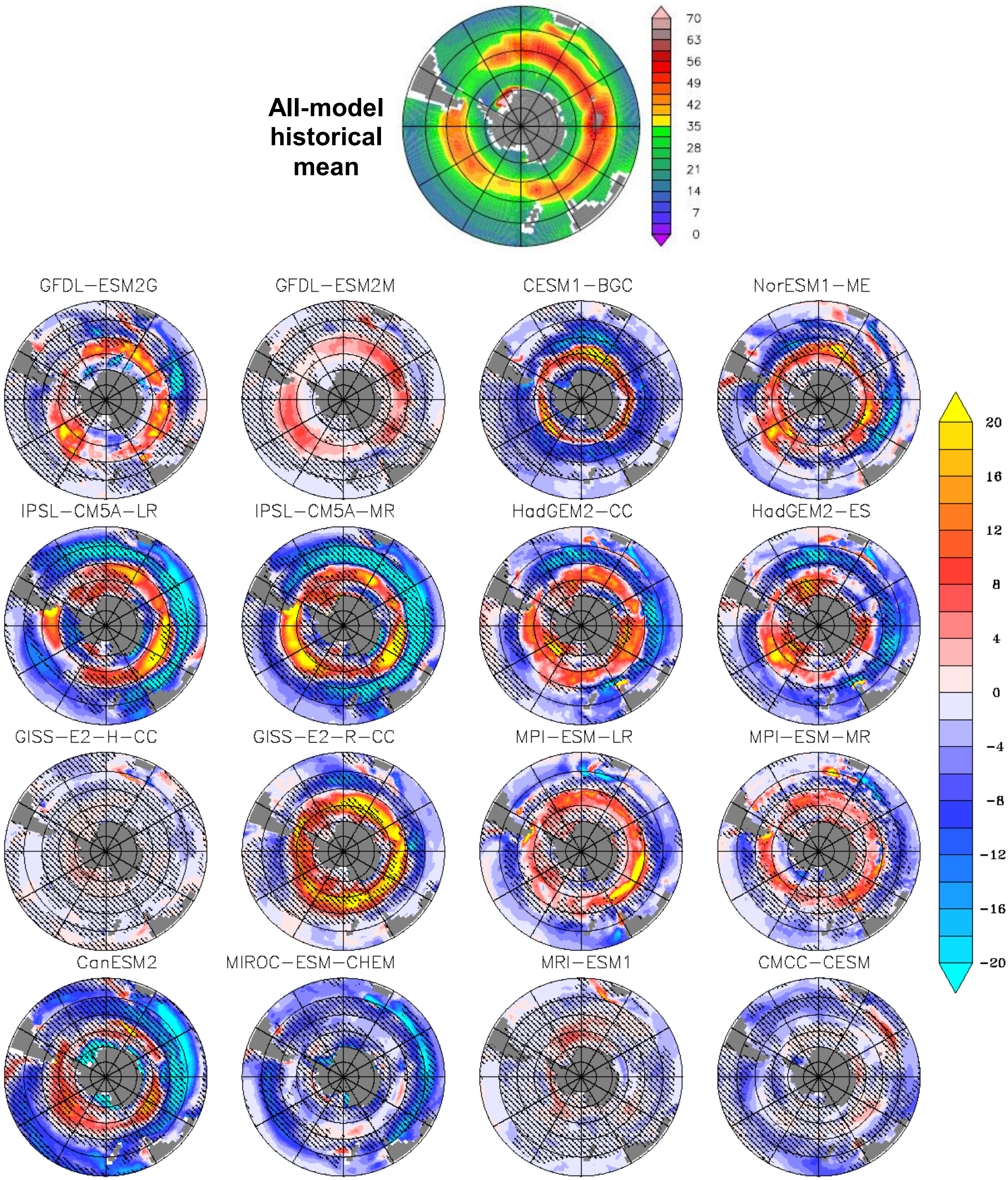

Figure S5: 100-year changes in minimum annual MLD for all the models with this data available. Shaded areas are where PP increases.

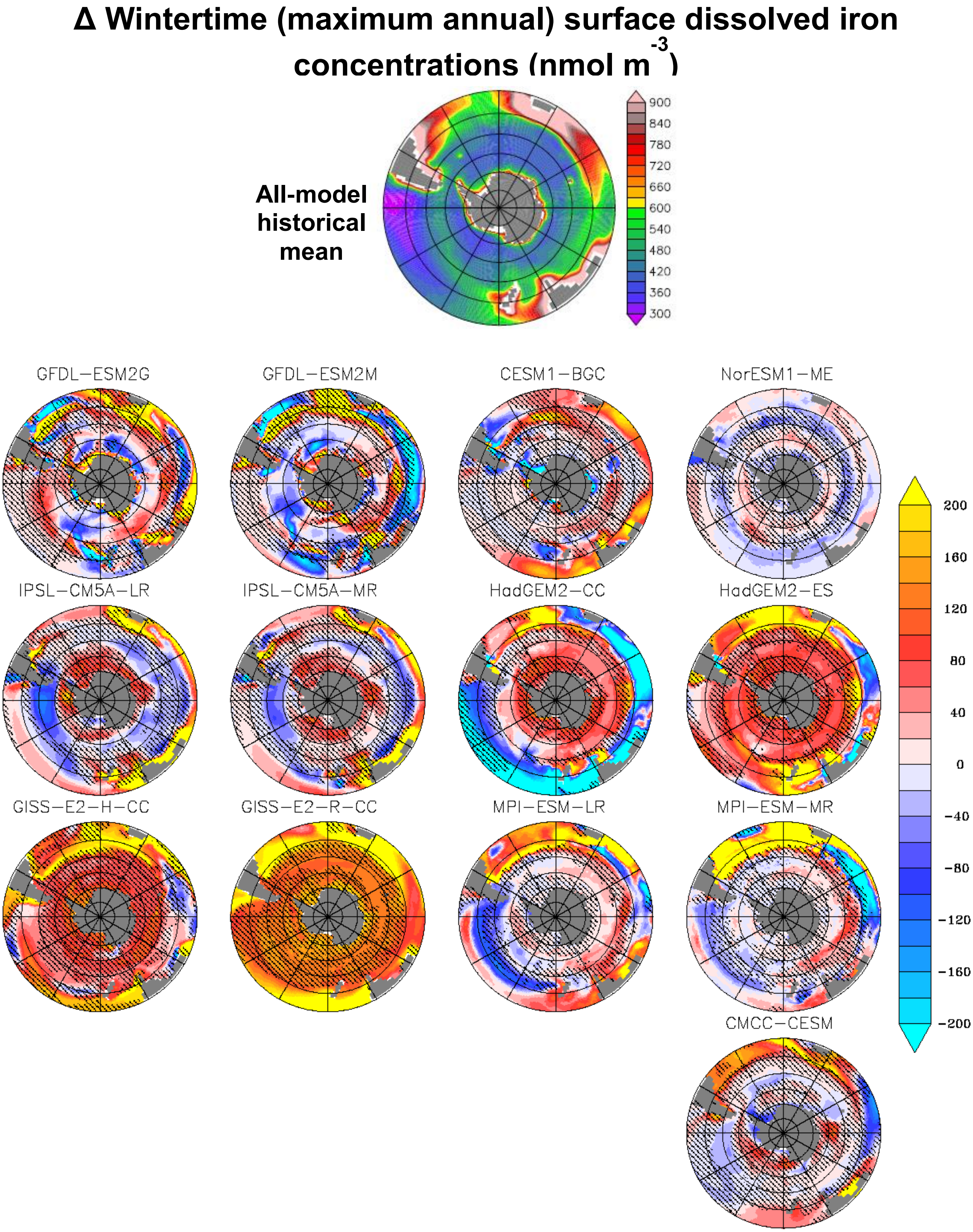

Figure S6: 100-year changes in maximum annual surface dissolved iron concentration for all the models with this data available. Shaded areas are where PP increases.

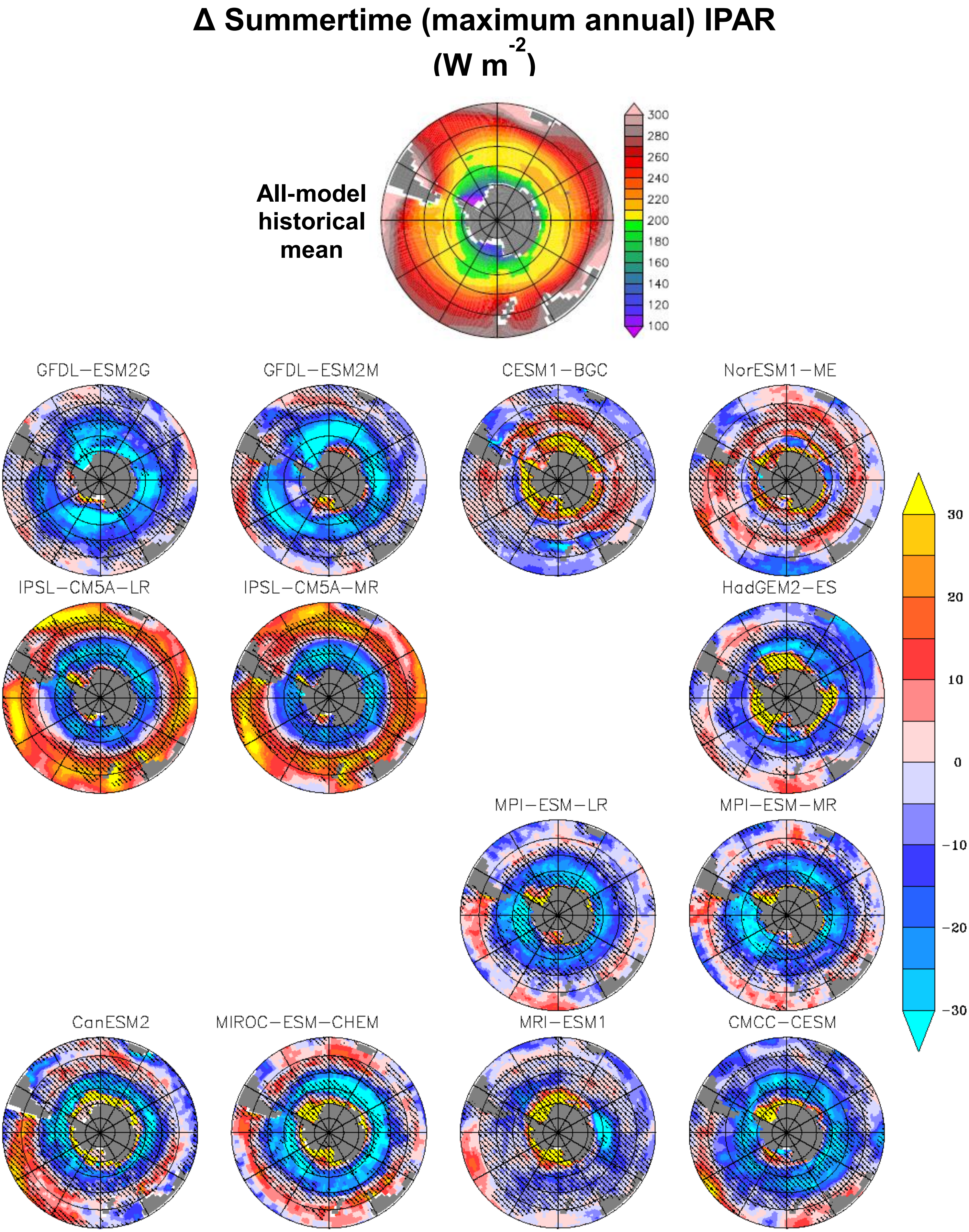

Figure S7: 100-year changes in maximum annual IPAR for all the models with this data available. Shaded areas are where PP increases.

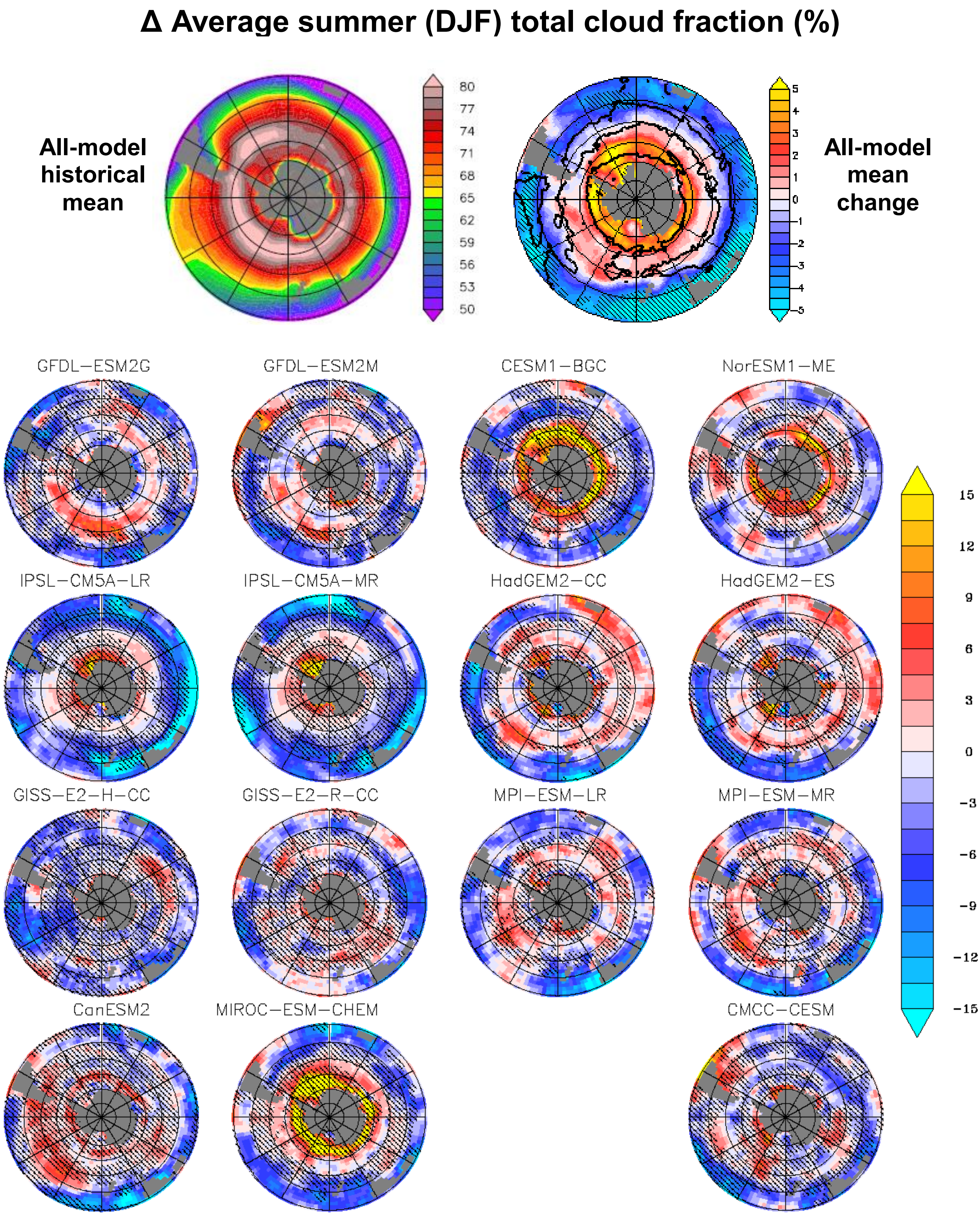

Figure S8: 100-year changes in average summer total cloud fraction for all the models with this data available. Shaded areas are where PP increases.

Δ Average annual zonal wind stress (Pa)

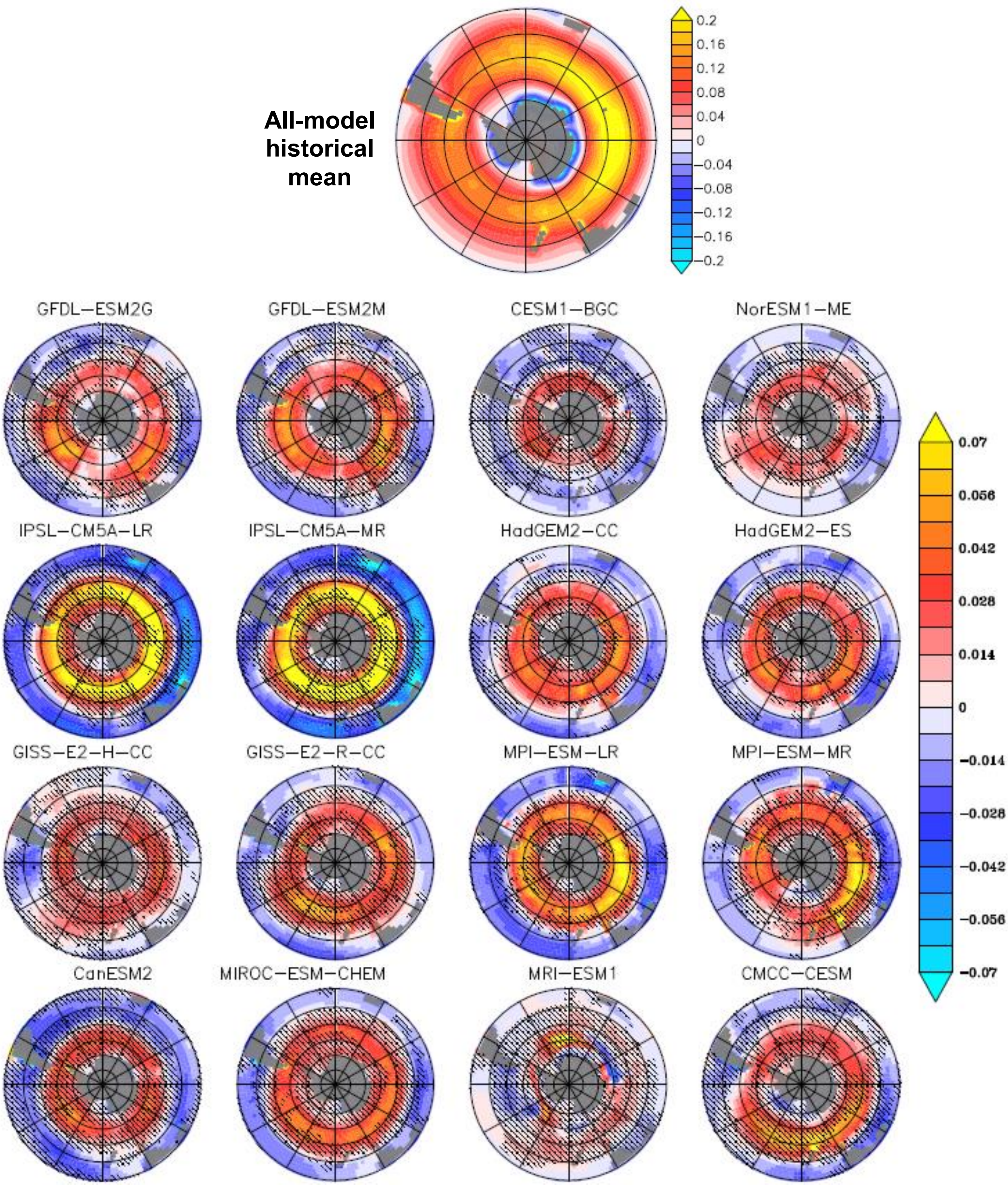

Figure S9: 100-year changes in average annual zonal wind stress for all the models with this data available. Shaded areas are where PP increases.

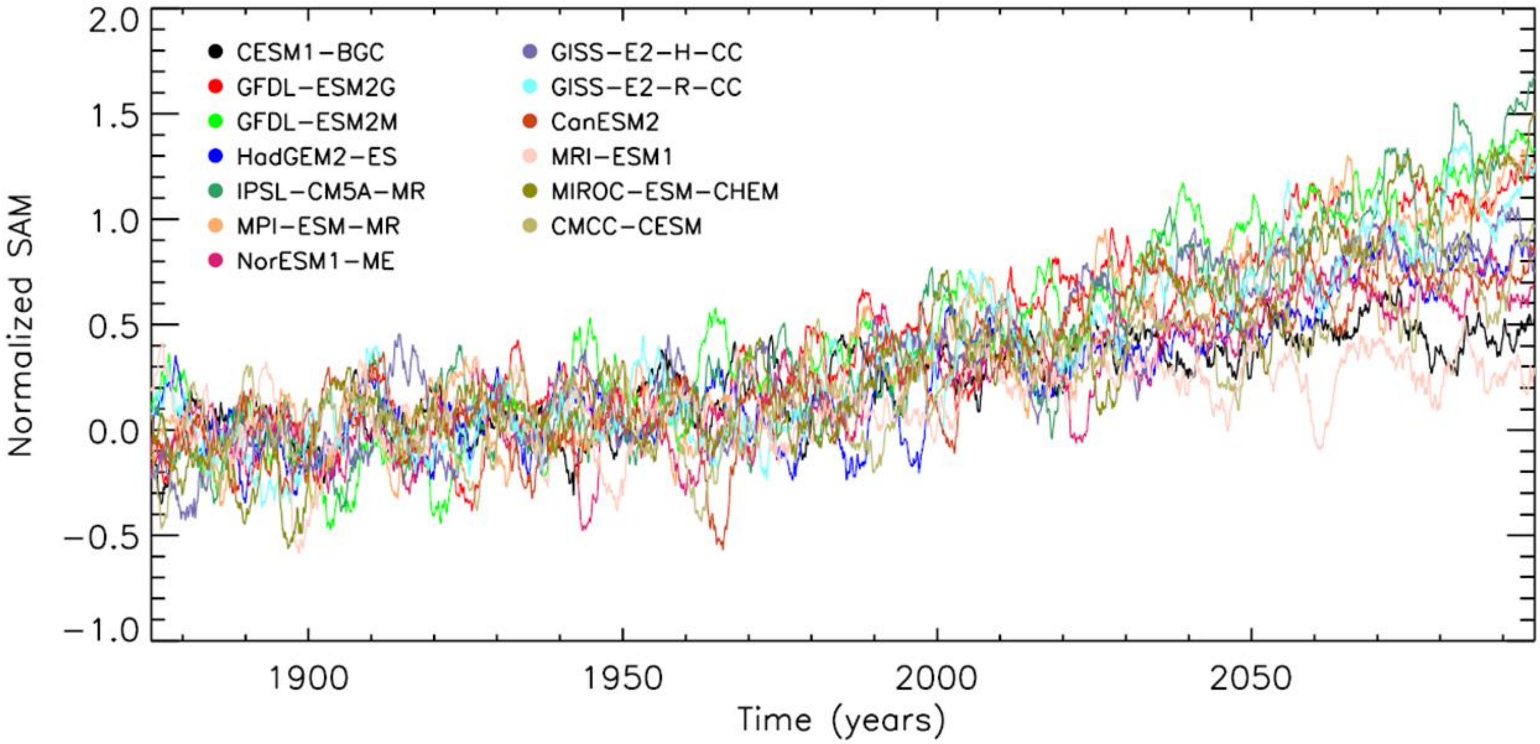

Fig. S10: Time series of the normalized Southern Annular Mode (SAM) index from the historical (1870-2005) and rcp8.5 (2006-2099) scenarios within each CMIP5 model studied here. The original SAM index time series is calculated as the difference between monthly zonally-averaged sea level pressure at 40°S and 60°S. To normalize, the average monthly SAM index between 1870 and 1950 is subtracted from the original SAM index time series at each month; this difference is then divided by the standard deviation of the SAM index between 1870 and 1950.

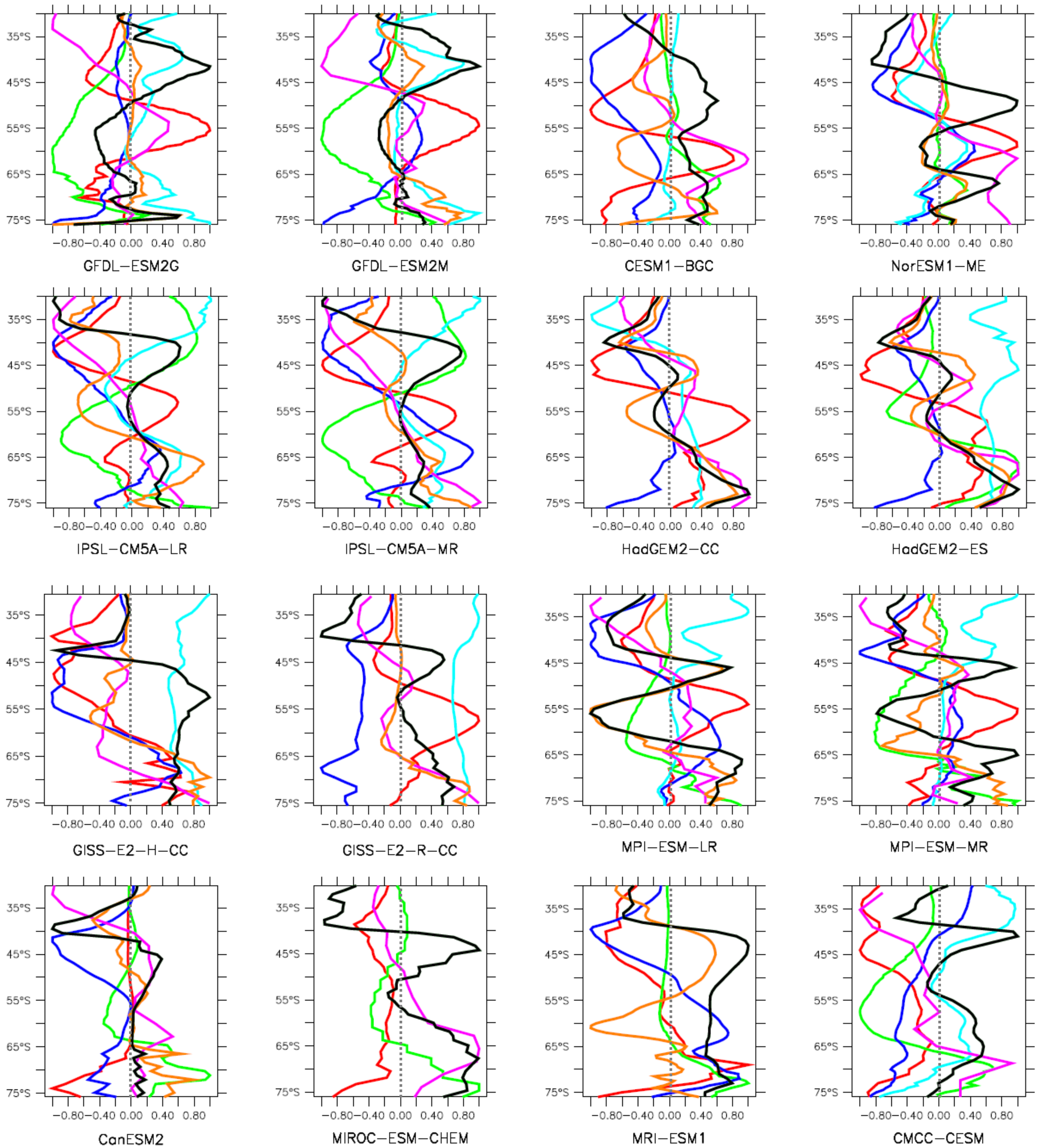

Fig. S11: Normalized zonally-averaged 100-year changes in PP, PB, and other variables of interest (analogous to Fig. 5, but with plots for each model individually). For each variable, normalization was achieved by first computing the mean zonally-averaged 100-year change within each of the models at every latitude and then dividing these values by the absolute value of the largest of these changes occurring south of 30°S. Some variables are omitted from some models due to lack of data. Plot colors are the same as in Fig. 5.

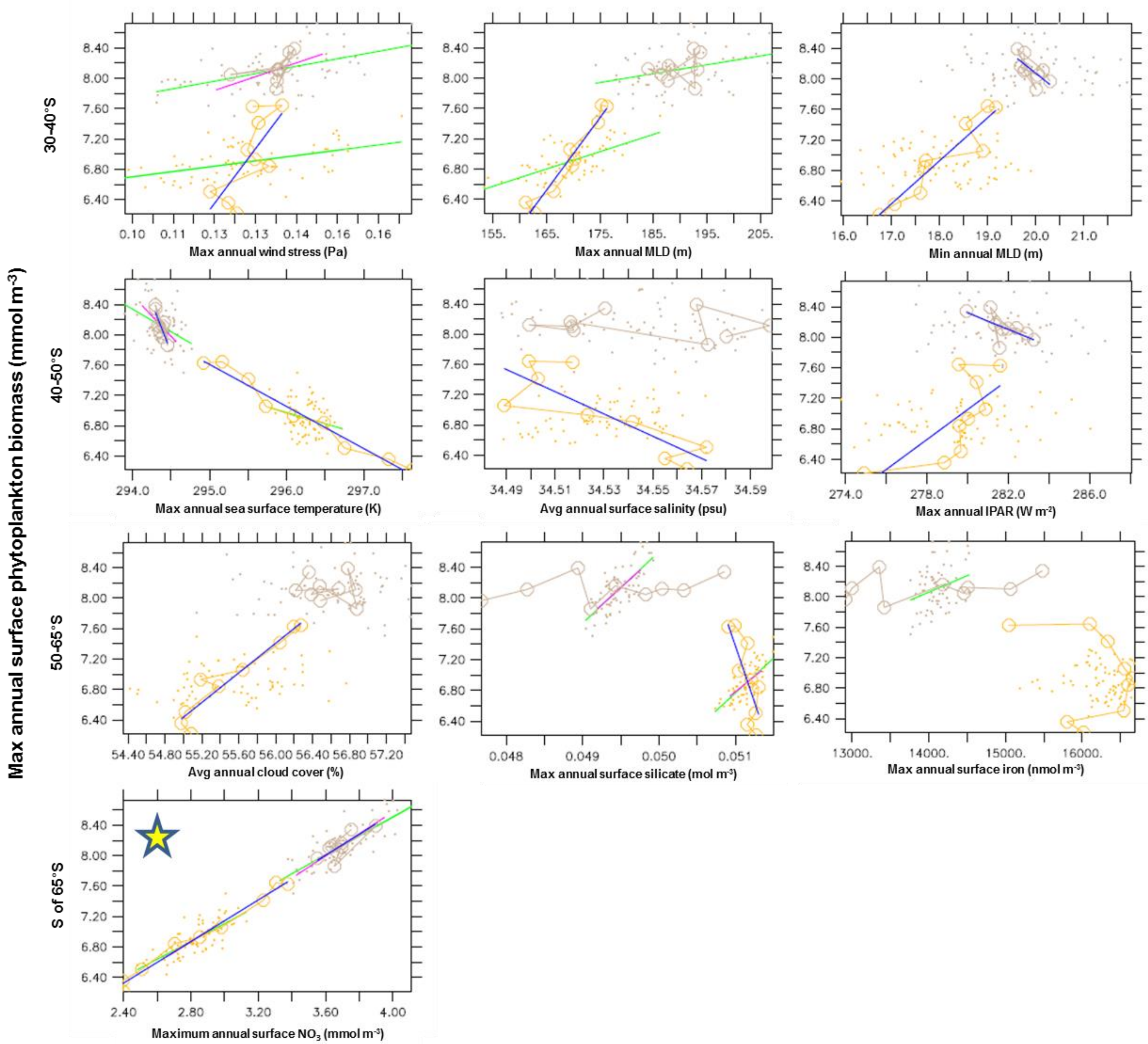

Fig. S12: Examples of temporal correlations between PB and variables which were not chosen for inclusion in Fig. 2, compared to correlations between PB and the variable which was chosen (starred). Here we plot correlations from model HadGEM2-ES's masked 30-40°S band, but other bands within other models show similar distinctively clear correlations between PB and the chosen driving variable. Plot legend is the same as in Fig. 2.

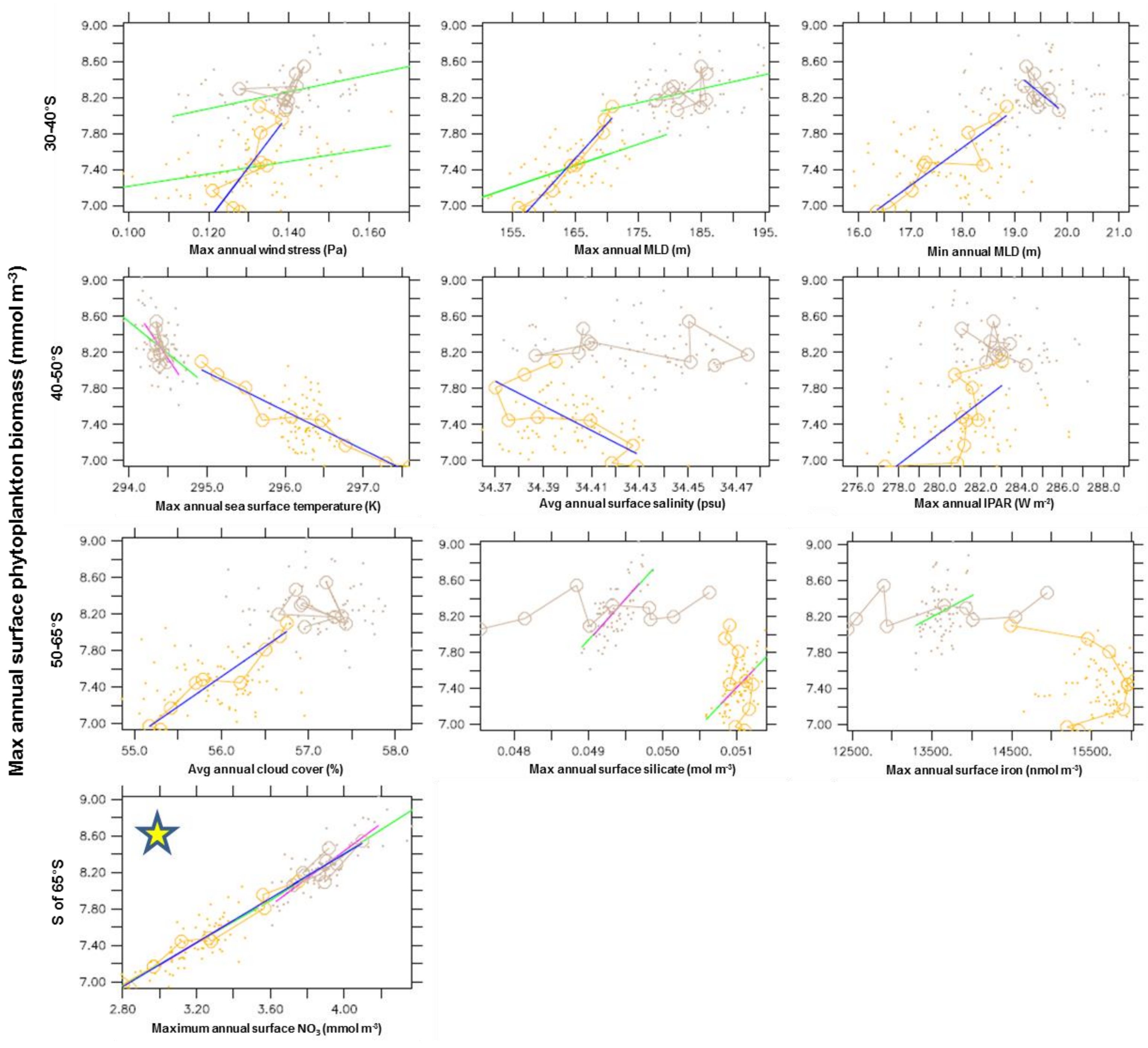

Fig. S13: As in Fig. S12, but showing temporal correlations from model HadGEM2-ES's unmasked 30-40°S band. Comparison to Fig. S12 suggests that masking does not significantly alter any results. Here we plot correlations from HadGEM2-ES, but other bands within other models show similarly minor sensitivities to masking. Plot legend is the same as in Fig. 2.

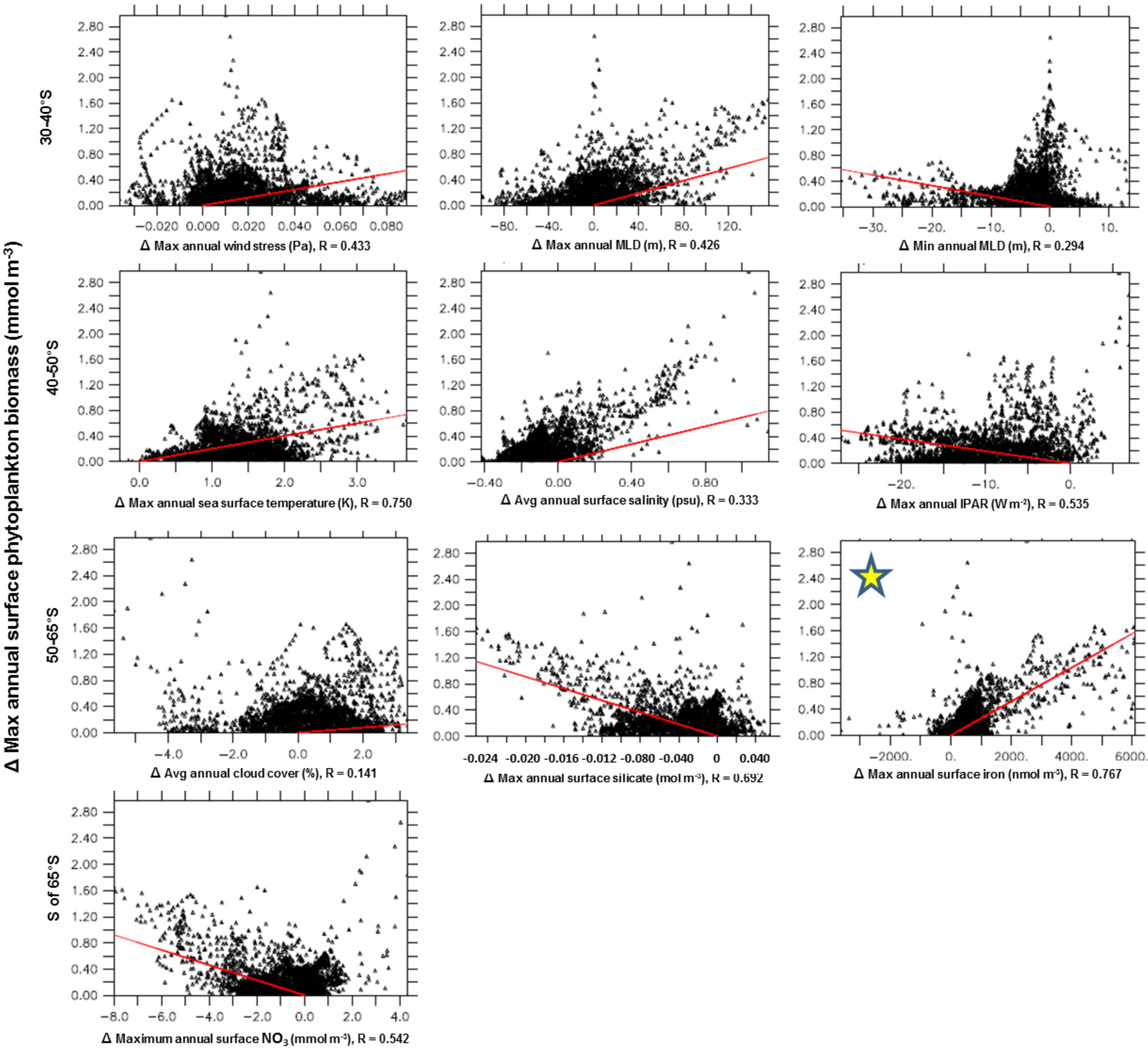

Fig. S14: Examples of spatial correlations between PB and variables which were not chosen for inclusion in Fig. 3, compared to correlations between PB and the variable which was chosen (starred). Here we plot correlations from model GFDL-ESM2G's masked 40-50°S band, but other bands within other models show similar distinctively clear correlations between PB and the chosen driving variable. Plot legend is the same as in Fig. 3.

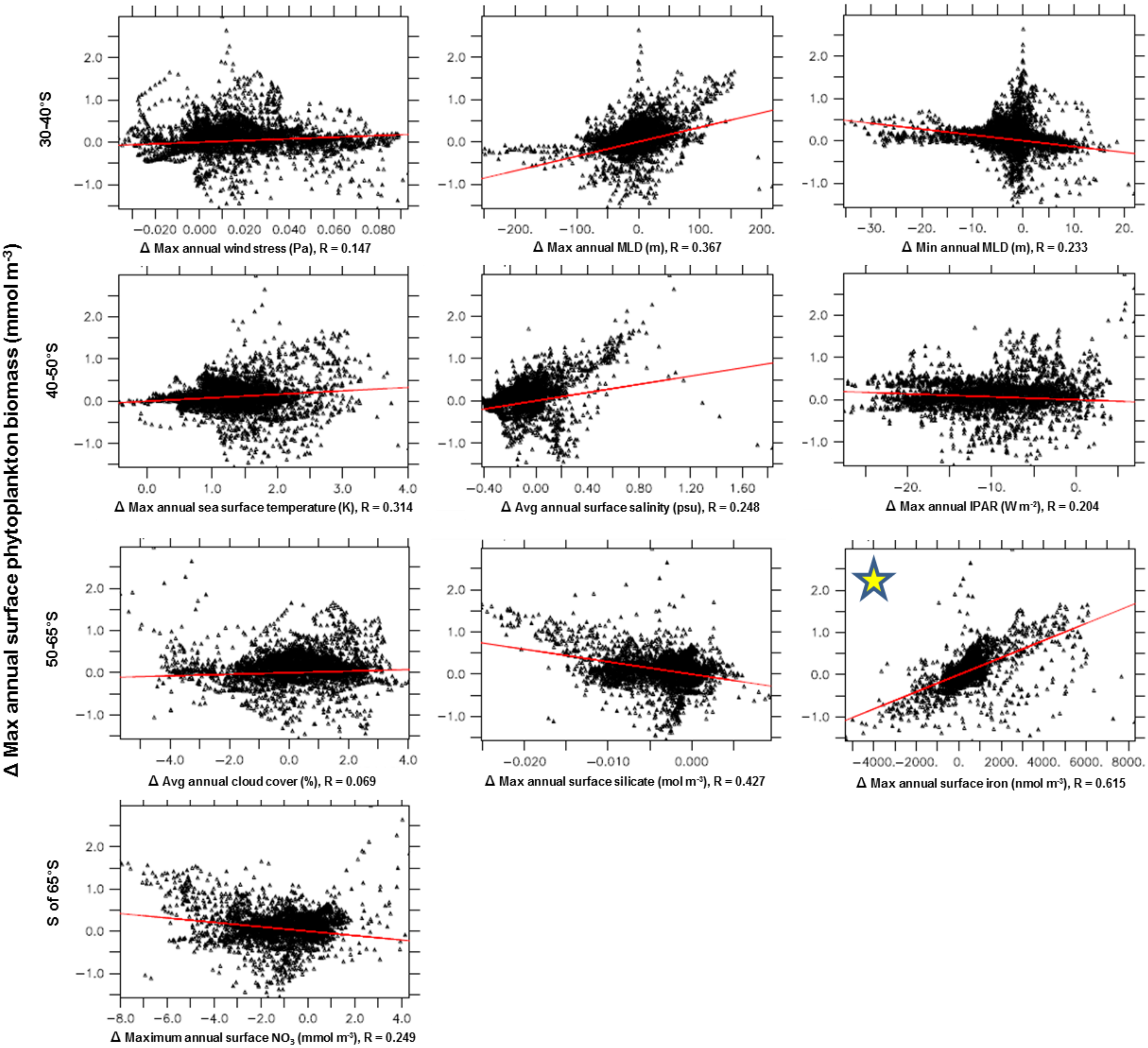

Fig. S15: As in Fig. S14, but showing spatial correlations from model GFDL-ESM2G's unmasked 40-50°S band. Comparison to Fig. S14 suggests that masking does not significantly alter any results. Here we plot correlations from GFDL-ESM2G, but other bands within other models show similarly minor sensitivities to masking. Plot legend is the same as in Fig. 3.

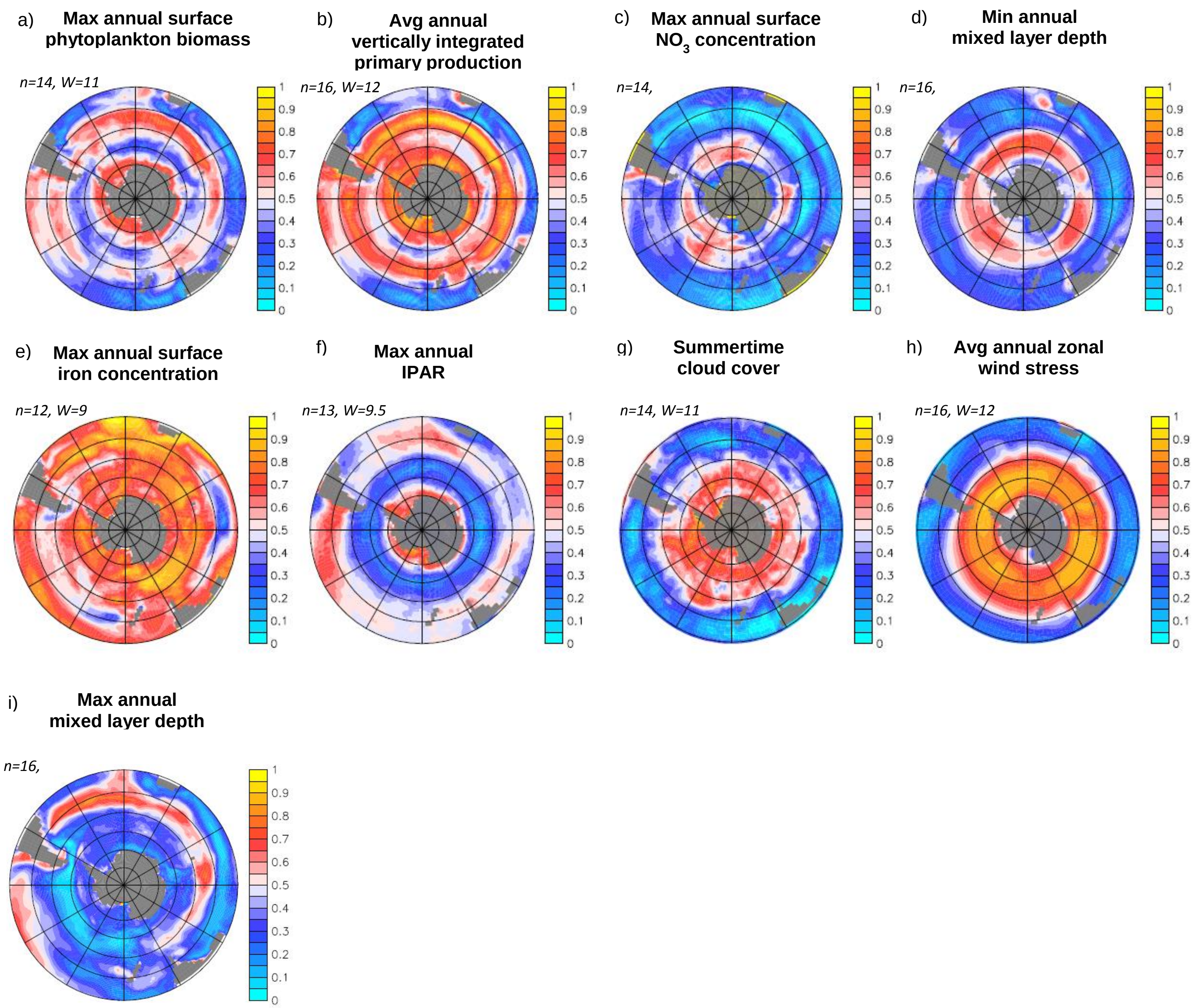

Fig. S16: Maps of the fraction of model realizations that agree on a positive 100-year change in variables of interest at each grid point, based on a bootstrap analysis test (see Sect. 2.4). The closer to 1 the grid point, the greater the agreement among models on an increase. The closer to 0 the grid point, the greater the agreement among models on a decrease.